The Astrophysical Journal Letters, 994:L8 (12pp), 2025 November 20 https://doi.org/10.3847/2041-8213/ae1837

Enabling Early Transient Discovery in LSST via Difference Imaging with DECam

Yize Dong (董一泽)[1,2], Kaylee de Soto[1], V. Ashley Villar[1,2], Anya Nugent[1], Alex Gagliano[1,2,3], K. Azalee Bostroem[4,33], Anastasia Alexov[5], Éric Aubourg[6], Farrukh Azfar[7], Alexandre Boucaud[8], Andrew Bradshaw[9,10], Johann Cohen-Tanugi[11], Sylvie Dagoret-Campagne[12], Philip Daly[4], Felipe Daruich[13], Peter E. Doherty[14], Holger Drass[13], Orion Eiger[9,10], Leanne P. Guy[13], Patrick A. Hascall[9], Željko Ivezić[5,15], Fabrice Jammes[11], M. James Jee[16,17], Tim Jenness[5], Steven M. Kahn[18], Yijung Kang[10,13], Lee S. Kelvin[19], Ivan V. Kotov[20], Gábor Kovács[21], Laurent Le Guillou[22], Shuang Liang[9], Mostafa Lutfi[5], Morgan May[20,23], Guillem Megias Homar[24], Marc Moniez[12], Freddy Muñoz Arancibia[5], Erfan Nourbakhsh[19], Hye Yun Park[25], John R. Peterson[26], Andrés A. Plazas Malagón[9,10], Daniel Polin[17], Bruno C. Quint[5], Tiago Ribeiro[5], Vincent J. Riot[27], Cécile Roucelle[8], Bruno O. Sánchez[28], David Sanmartim[13], Jacques Sebag[13], Nima Sedaghat[15], Richard A. Shaw[29], Alysha Shugart[13], Ioana Sotuela Elorriaga[13], Krzysztof Suberlak[15], John D. Swinbank[19,30], Sandrine Thomas[5], J. Anthony Tyson[17], Wouter van Reeven[13], Charlotte Ward[31], Christopher Z. Waters[19], Oliver Wiecha[5], and W. M. Wood-Vasey[32]

[1] Center for Astrophysics | Harvard & Smithsonian, Cambridge, MA 02138, USA; yize.dong@cfa.harvard.edu
[2] The NSF AI Institute for Artificial Intelligence and Fundamental Interactions, USA
[3] Department of Physics and Kavli Institute for Astrophysics and Space Research, Massachusetts Institute of Technology, 77 Massachusetts Avenue, Cambridge, MA 02139, USA
[4] Steward Observatory, University of Arizona, 933 N. Cherry Avenue, Tucson, AZ 85721-0065, USA
[5] Vera C. Rubin Observatory Project Office, 950 N. Cherry Avenue, Tucson, AZ 85719, USA
[6] Université Paris Cité, CNRS/IN2P3, CEA, APC, 4 rue Elsa Morante, F-75013 Paris, France
[7] Department of Physics, University of Oxford, Denys Wilkinson Building, Keble Road, Oxford, OX1 3RH, UK
[8] Université Paris Cité, CNRS/IN2P3, APC, 4 rue Elsa Morante, F-75013 Paris, France
[9] SLAC National Accelerator Laboratory, 2575 Sand Hill Road, Menlo Park, CA 94025, USA
[10] Kavli Institute for Particle Astrophysics and Cosmology, SLAC National Accelerator Laboratory, 2575 Sand Hill Road, Menlo Park, CA 94025, USA
[11] Université Clermont Auvergne, CNRS/IN2P3, LPCA, 4 Avenue Blaise Pascal, F-63000 Clermont-Ferrand, France
[12] Université Paris-Saclay, CNRS/IN2P3, IJCLab, 15 Rue Georges Clemenceau, F-91405 Orsay, France
[13] Vera C. Rubin Observatory, Avenida Juan Cisternas #1500, La Serena, Chile
[14] Smithsonian Astrophysical Observatory, 60 Garden Street, Cambridge, MA 02138, USA
[15] University of Washington, Dept. of Astronomy, Box 351580, Seattle, WA 98195, USA
[16] Department of Astronomy, Yonsei University, 50 Yonsei-ro, Seoul 03722, Republic of Korea
[17] Physics Department, University of California, One Shields Avenue, Davis, CA 95616, USA
[18] Physics Department, University of California, 366 Physics North, MC 7300 Berkeley, CA 94720, USA
[19] Department of Astrophysical Sciences, Princeton University, Princeton, NJ 08544, USA
[20] Brookhaven National Laboratory, Upton, NY 11973, USA
[21] Institute for Data-intensive Research in Astrophysics and Cosmology, University of Washington, 3910 15th Avenue NE, Seattle, WA 98195, USA
[22] Sorbonne Université, Université Paris Cité, CNRS/IN2P3, LPNHE, 4 place Jussieu, F-75005 Paris, France
[23] Department of Physics Columbia University, New York, NY 10027, USA
[24] Division of Physics, Mathematics and Astronomy, California Institute of Technology, Pasadena, CA 91125, USA
[25] Department of Physics, Duke University, Durham, NC 27708, USA
[26] Department of Physics and Astronomy, Purdue University, 525 Northwestern Avenue, West Lafayette, IN 47907, USA
[27] Lawrence Livermore National Laboratory, 7000 East Avenue, Livermore, CA 94550, USA
[28] Aix Marseille Université, CNRS/IN2P3, CPPM, 163 avenue de Luminy, F-13288 Marseille, France
[29] Space Telescope Science Institute, 3700 San Martin Drive, Baltimore, MD 21218, USA
[30] ASTRON, Oude Hoogeveensedijk 4, 7991 PD, Dwingeloo, The Netherlands
[31] Department of Astronomy and Astrophysics, The Pennsylvania State University, 525 Davey Lab, University Park, PA 16802, USA
[32] Department of Physics and Astronomy, University of Pittsburgh, 3941 O'Hara Street, Pittsburgh, PA 15260, USA
Received 2025 August 11; revised 2025 October 23; accepted 2025 October 24; published 2025 November 11

Abstract

We present SLIDE, a pipeline that enables transient discovery in data from the Vera C. Rubin Observatory's Legacy Survey of Space and Time (LSST), using archival images from the Dark Energy Camera as templates for difference imaging. We apply this pipeline to the recently released Data Preview 1 (DP1; the first public release of Rubin commissioning data) and search for transients in the resulting difference images. The image subtraction, photometry extraction, and transient detection are all performed on the Rubin Science Platform. We demonstrate that SLIDE effectively extracts clean photometry by circumventing poor or missing LSST templates. We identified 29 previously unreported transients, 12 of which would not have been detected based on the DP1 DiaObject catalog. SLIDE will be especially useful for transient analysis in the early years of LSST, when

[33] LSSTC Catalyst Fellow.

template coverage will be largely incomplete or when templates may be contaminated by transients present at the time of acquisition. We present multiband light curves for a sample of known transients, along with new transient candidates identified through our search. Finally, we discuss the prospects of applying this pipeline during the main LSST survey. Our pipeline is broadly applicable and will support studies of all transients with slowly evolving phases.

Unified Astronomy Thesaurus concepts: Core-collapse supernovae (304); Supernovae (1668); Transient detection (1957)

Materials only available in the online version of record: data behind figures

1. Introduction

The wide field of view and exceptional depth of the Vera C. Rubin Observatory will usher in a new era for time-domain astronomy (LSST Science Collaboration et al. 2009). Expected to begin full operations in late 2025, the Rubin Observatory's decade-long Legacy Survey of Space and Time (LSST; Ž. Ivezić et al. 2019) will stream up to 10 million transient alerts nightly. Data taken between 2023 November 4 and 2024 December 10 with the LSST Commissioning Camera ("LSSTComCam"), which uses the same hardware as the LSST Camera but with a reduced field of view (SLAC National Accelerator Laboratory & NSF-DOE Vera C. Rubin Observatory 2025), were released as Data Preview 1 (DP1;[34] SLAC National Accelerator Laboratory & NSF-DOE Vera C. Rubin Observatory 2024; NSF-DOE Vera C. Rubin Observatory 2025a, 2025b).

LSST's nightly alerts rely on difference imaging, which compares new observations to deep reference templates to identify brightness fluctuations from variable and transient sources. Template collection is expected to continue through the first year of regular survey operations (L. P. Guy et al. 2023, 2025). Transients observed during this early period may contaminate templates, making it difficult to accurately distinguish their flux from contaminating background light (e.g., from the host galaxy). Such contamination may not significantly affect the transient detections for rapidly evolving transients or supernovae (SNe) that change brightness on relatively short timescales. Despite inaccurate reported photometry, these transients can still be detected by the LSST alert stream even if partially imprinted in the templates.

In contrast, long-duration transients that do not exhibit strong luminosity evolution will be difficult to identify in real time if they are present in the LSST templates. This includes long-lived precursors to core-collapse SNe (CCSNe; A. Pastorello et al. 2007; N. L. Strotjohann et al. 2021; D. Tsuna et al. 2023, 2024a; S. J. Brennan et al. 2025) such as those detected in SN 2020tlf (W. V. Jacobson-Galán et al. 2022), SN 2023fyq (S. J. Brennan et al. 2024; Y. Dong et al. 2024), SN 2023zkd (A. Gagliano et al. 2025), as well as long-duration superluminous SNe (e.g., S. Gomez et al. 2024) and luminous red novae (LRNe; J. C. Mauerhan et al. 2015; N. Smith et al. 2016; N. Blagorodnova et al. 2017). Even if such transients are detected, obtaining clean photometry will require waiting until they have faded, at which point templates can be constructed. This delay could hinder timely follow-up and downstream analysis during the early phases of the LSST survey.

The release of Rubin DP1 provides a valuable dataset for developing and testing infrastructure that can be applied to real LSST data. In this Letter, we present the `SLIDE` package for performing LSST image subtraction using images taken by the Dark Energy Camera (DECam; K. Honscheid & D. L. DePoy 2008; B. Flaugher et al. 2015). This provides an alternative to LSST-derived templates and will benefit the broader transient community in the initial years of the LSST survey.

We have released our `SLIDE` package on GitHub.[35] `SLIDE` is intended to be run directly on the Rubin Science Platform (G. Dubois-Felsmann et al. 2019; W. O'Mullane et al. 2024). We use `SLIDE` to search for DP1 transients within two of the extragalactic fields observed by LSSTComCam: the Extended Chandra Deep Field South (ECDFS) and the Euclid Deep Field South (EDFS). We find that all transients reported to the Transient Name Server (TNS; A. Gal-Yam 2021) within our selected search area are successfully recovered, provided they had not already faded by the time the images were taken. In addition, we identify 29 previously unreported transients, 18 of which are likely nuclear transients, and 12 of which are either not present or have fewer than two detections in DP1's `DiaObject` catalog (NSF-DOE Vera C. Rubin Observatory 2025c).

In Section 2, we provide an overview of `SLIDE` and test it on a Rubin LSSTComCam transient with template contamination. In Section 3, we describe our search for transient candidates in the EDFS and ECDFS fields using our corrected difference images. We summarize our findings and outline future prospects with the full LSST data stream in Section 4.

2. LSST Image Subtraction with `SLIDE`

`SLIDE` can be easily installed on the Rubin Science Platform[36,37] (W. O'Mullane et al. 2024). We include an example notebook to demonstrate its usage.[38] Here, we outline its major components.

DECam is a wide-field charge-coupled device (CCD) imager mounted on the 4 m Blanco telescope at Cerro Tololo Inter-American Observatory (CTIO) in northern Chile. Initially designed for the Dark Energy Survey (DES; Dark Energy Survey Collaboration et al. 2016), DECam consists of 62 science CCDs with a pixel scale of $0.''263$ pixel^{-1} and a field of view of approximately 3 deg^2. The DES survey was conducted from 2013 August 15 to 2019 January 9 and covered 5000 deg^2 in *grizY* bands.

`SLIDE` automatically retrieves deep coadded images from the DES Data Release 2 (DR2; T. M. C. Abbott et al. 2021) that overlap a position of interest. The final coadds reach a median 5σ depth of $g = 25.4$, $r = 25.1$, $i = 24.5$, $z = 23.8$, and

[34] https://rtn-095.lsst.io

[35] https://github.com/yizedong/SLIDE

[36] https://ldm-542.lsst.io

[37] https://lse-319.lsst.io

[38] https://github.com/yizedong/SLIDE/blob/main/example.ipynb

$Y = 22.4$, which are deeper than single-visit depths expected from LSST and deeper than images released as part of DP1 (F. B. Bianco et al. 2022; NSF-DOE Vera C. Rubin Observatory 2025b). This makes DES DR2 images suitable as templates for LSST image subtraction. All the difference images used in this Letter are made using the DES DR2 templates.

Alternatively, `SLIDE` can retrieve coadded DECam images from the Dark Energy Camera Legacy Survey (DECaLS; R. D. Blum et al. 2016; A. Dey et al. 2019) for use as templates. These images have similar or slightly greater depth than single exposures in DP1, making them a useful alternative when DES templates are not available. Users may also supply custom DECam templates.

DES DR2 (or DECaLS) images are retrieved using the Simple Image Access service provided by the Astro Data Lab (M. J. Fitzpatrick et al. 2014; R. Nikutta et al. 2020). DECam images are aligned and rescaled to match the LSST images using the `reproject` package,[39] which uses an adaptive, antialiased resampling algorithm (C. E. DeForest 2004). The point-spread function (PSF) of the DECam images is modeled using `Photutils` with stars selected from the Gaia DR3 catalog (Gaia Collaboration et al. 2016, 2021; M. Riello et al. 2021).

For DP1 images, we obtain the calibrated exposure images (`visit_image`) from the Rubin Science Platform using the Butler (T. Jenness et al. 2022). These images have been processed by the LSST Science Pipelines (Rubin Observatory Science Pipelines Developers 2025) and are ready for scientific use. LSSTComCam consists of nine CCDs; `SLIDE` can operate on either full CCD images or cutout regions. The LSSTComCam image PSFs provided can vary slightly over the field of view. Therefore, we use the median PSF of the detector for image subtraction. Alternatively, our package offers options to recalculate the PSF and refine the World Coordinate System of images using stars from Gaia DR3.

The image subtraction is performed using a Python implementation of the Zackay–Ofek–Gal-Yam (ZOGY; B. Zackay et al. 2016; D. Guevel & G. Hosseinzadeh 2017) algorithm,[40] which provides mathematically optimal statistics for image subtraction and does not require that the reference image has a sharper PSF than the science image. The runtime for PSF construction and image subtraction depends on image size: for a full LSST CCD image (4000×4000 pixels), it takes approximately 1.5 minutes, while for a 1500×1500 pixel cutout, it takes about 15 s.

Finally, PSF photometry is performed on the difference images at specified positions (R.A. and decl.) using the `Photutils` package from `astropy` (Astropy Collaboration et al. 2022).

We test `SLIDE` on a known transient, AT 2024ahzi, which was reported to TNS on 2025 March 13 (I. Andreoni et al. 2025; C. T. Murphey et al. 2025). Flux from AT 2024ahzi is present in the LSSTComCam templates used by DP1, making the reported difference-imaged forced photometry unreliable (K. de Soto 2025, in preparation). We process all available DES images overlapping the transient position and find that the resulting photometry is consistent with that obtained by the Young Supernova Experiment (D. O. Jones et al. 2021; P. D. Aleo et al. 2023) using DECam within $\sim 1\sigma$ (see detailed photometric comparison in K. de Soto 2025, in preparation). In Figure 1, we show examples of image subtraction at the position of AT 2024ahzi using the DES templates as a demonstration of the subtraction quality. The subtractions are generally clean, and the transient is clearly detected in the center when present.

3. Candidate Transients Search

3.1. Field Selection

Rubin DP1 contains *ugrizy* images from seven fields, taken with LSSTComCam between 2024 November and December. We select the ECDFS and the EDFS fields to perform an experimental transient search, as these are the most well-observed fields in DP1, are far from the Galactic plane, and have sufficiently overlapping coverage by DES. For each field, we select a subset of *r*-band exposures that maximizes overall spatial overlap across visits while also ensuring even temporal coverage. We restrict the transient search to a single filter to reduce the computational workload; we prefer the *r* band as it has the highest cadence in both fields. This selection yields 37 visits of ECDFS and 18 visits of EDFS. For each visit, image subtraction is performed on each CCD's image independently.

3.2. Transient Detection

Transient detection is performed on the difference images using `SEP` (K. Barbary 2016), a Python implementation of Source Extractor (E. Bertin & S. Arnouts 1996).

Stars brighter than approximately 16 mag saturate LSSTComCam's 30 s exposures. Although these bright stars are masked out in the difference images, we find that they often produce prominent spike-like artifacts in the surrounding area, which can be misidentified as transient detections. To mitigate contamination, we exclude any candidates located within 20″ of such stars. Additionally, we find that stars with proper motion may be misaligned between the template and science images. Such misalignment can create residual artifacts in the difference images, and we therefore exclude candidates located within one full width at half-maximum of sources classified as stars in the DES DR2 catalog (T. M. C. Abbott et al. 2021).

To identify transients of interest from the remaining 15,785 targets, we require that each candidate has at least three detections, which removes contamination from cosmic rays and other artifacts. We also require that the peak-to-peak flux variation exceed 3 times the mean flux uncertainty, that the standard deviation of the flux exceed the mean flux uncertainty, and that the peak-to-peak magnitude variation be greater than 0.3 mag. Sources that do not meet all of these criteria are excluded from further analysis.

We associate the remaining 1224 candidates with likely host galaxies using `Pröst`[41] (A. Gagliano et al. 2025). `Pröst` calculates the posterior probability that each galaxy in a given search region is the true host galaxy using the fractional offset, redshift, and brightness of the host/transient. We use a search radius of 60" and consider galaxies in the *Galaxy List for Advanced Detector Era* catalog (GLADE; G. Dálya et al. 2022), Panoramic Survey Telescope and Rapid Response System (Pan-STARRS; K. C. Chambers et al. 2016) Data

[39] https://github.com/astropy/reproject
[40] https://github.com/dguevel/PyZOGY
[41] https://github.com/alexandergagliano/Prost

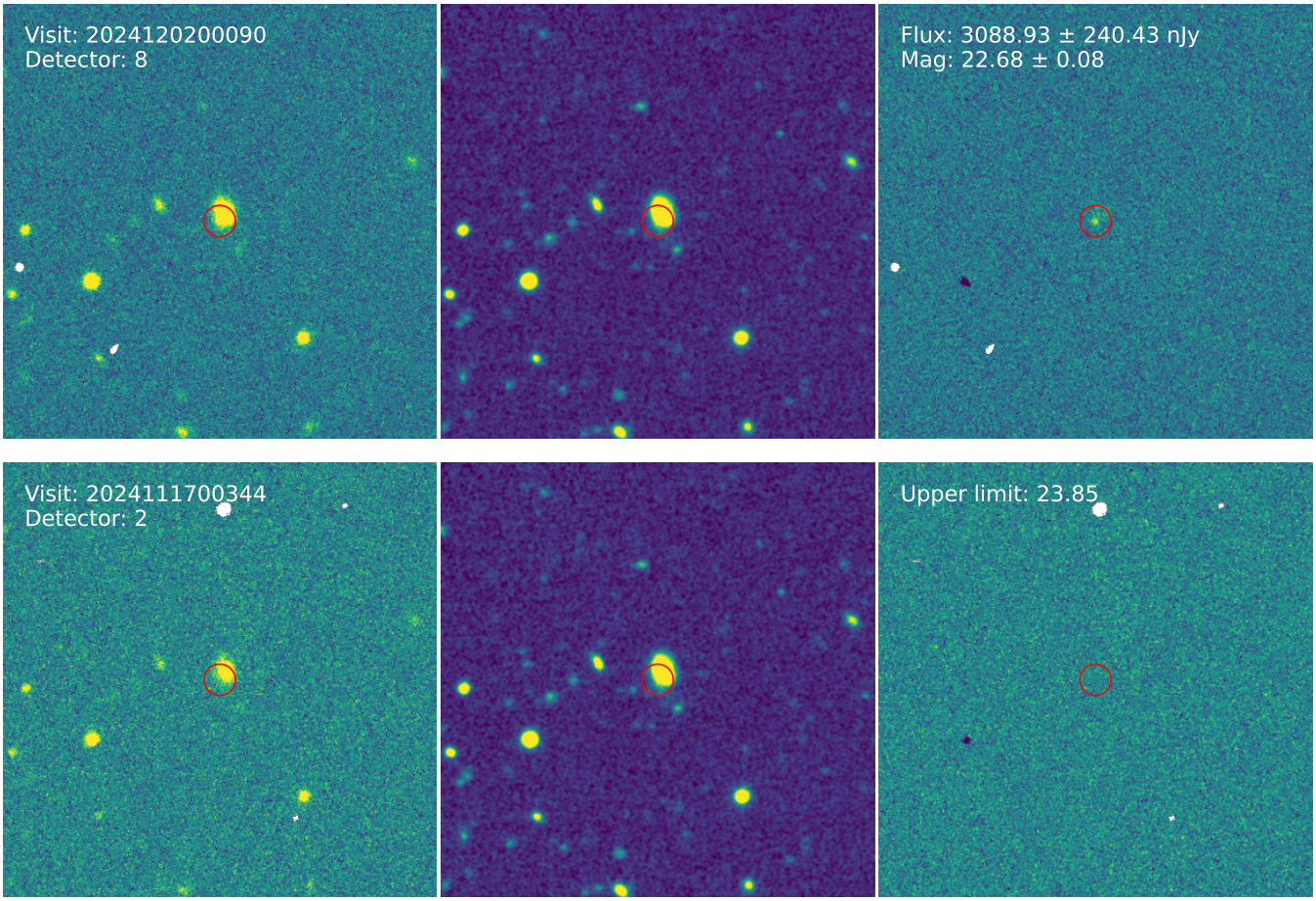

Figure 1. Upper: image subtraction using DECam templates for visit 2024120200090, detector 8, taken on 2024 December 2 in the *r* band. The image is oriented with north at the top and east to the left. AT 2024ahzi is visible on the image and marked by the red circle. The left and middle panels show the LSST image and the coadded DECam image, respectively, while the right panel shows the difference image. The displayed cutouts are 400 × 400 pixels in size, centered on the transient position. The white patches are bad pixels and are masked out prior to subtraction. PSF photometry is performed at the location of AT 2024ahzi on the difference image (center), and the results are annotated on the panel. Lower: image subtraction for visit 2024111700344, detector 2, taken on 2024 November 17 in the *r* band. AT 2024ahzi is not visible on the difference image, and an upper limit is derived.

Release 2 (DR2; H. A. Flewelling et al. 2020), and the DeCaLS Data Release 10. We also flag nuclear transients using `iinuclear`[42] (S. Gomez 2024), which determines whether the location of the transient coincides with the center of its host galaxy with sufficient probability. In our final candidate selection, we perform human vetting to select the most promising candidates and retain only transients, both nuclear and non-nuclear, with confident host associations.

Our criteria yield 39 transient candidates: 22 in ECDFS and 17 in EDFS. The detections for these candidates are separated by at least 20 days, which effectively excludes moving objects. These candidates are listed in Tables 1 and 2, respectively.

3.3. A Sample of Transient Light Curves in DP1

3.3.1. Known Transients

I. Andreoni et al. (2025) reported three newly identified extragalactic transient candidates and eight previously reported transients as visible in the DP1 images. These transients were required to have confident host galaxy associations and not to be colocated with star-like objects or galactic nuclei. Among the seven reported transients in the ECDFS/EDFS fields, AT 2024aigg (J. Freeburn et al. 2025e), AT 2024ahzc (C. T. Murphey et al. 2025), AT 2024ahyy (C. T. Murphey et al. 2025), and AT 2024aigk (A. Anumarlapudi et al. 2025) are successfully identified by our search algorithm. AT 2024ahzi (C. T. Murphey et al. 2025), AT 2024aigl (A. Anumarlapudi et al. 2025), and AT 2024ahwk (C. T. Murphey et al. 2025) are not identified because they were not covered by the selected visits used in the transient search. Had they been observed during the visits we selected, our algorithm would have robustly identified them.

We cross-match the remaining candidates with TNS, and we identify eight additional reported transients: six in the ECDFS field and two in the EDFS field. These transients are AT 2024aigs (J. Freeburn et al. 2025a), AT 2024aigh (J. Freeburn et al. 2025f), AT 2024aigt (J. Freeburn et al. 2025b), AT 2024aigw (J. Freeburn et al. 2025c), and AT 2024aigj (J. Freeburn et al. 2025g). We also note that AT 2024aigv (J. Freeburn et al. 2025c), AT 2024ahyq (C. T. Murphey et al. 2025), and AT 2024ahsx (C. T. Murphey et al. 2025) lie within the field we selected but are not detected, as they have fewer than three detections in our selected visits. We note that the photometric classifications of these TNS transients have been discussed in J. Freeburn et al. (2025d), and refer the reader to that work for further details.

[42] https://github.com/gmzsebastian/iinuclear

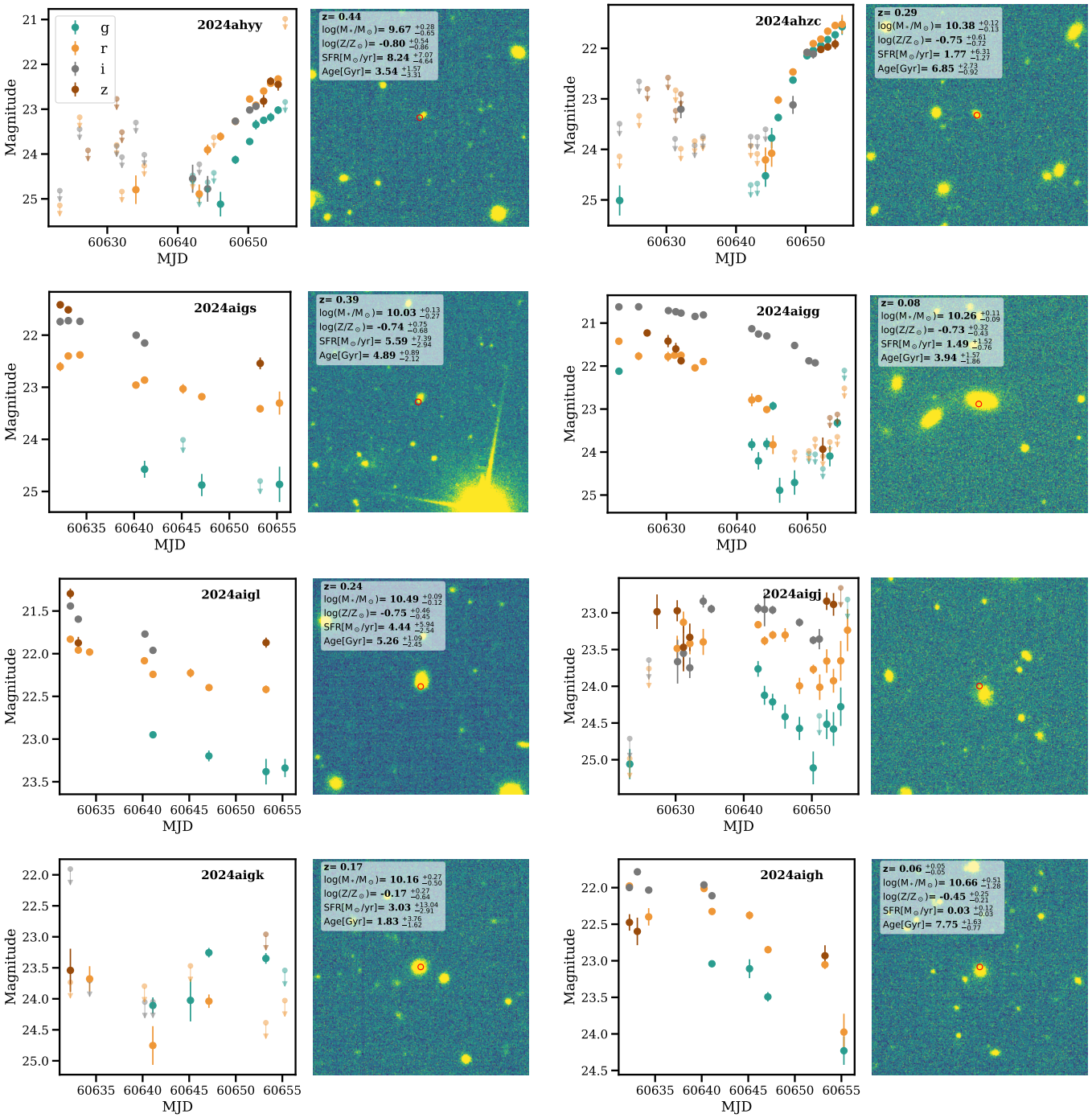

Figure 2. Light curves and host properties of transients previously reported to TNS. Note that plotted errors represent statistical uncertainty. Host properties include redshift (z), stellar mass ($\log(M_\star/M_\odot)$), stellar metallicity ($\log(Z/Z_\odot)$), star formation rate (SFR; ($M_\odot$, yr^{-1})), and mass-weighted stellar population age (Age; (Gyr)).

(The data used to create this figure are available in the online article.)

We perform PSF photometry using SLIDE at the positions of AT 2024ahyy, AT 2024ahzc, AT 2024aigs, AT 2024aigg, AT 2024aigl, AT 2024aigj, AT 2024aigk, AT 2024aigh, AT 2024aigw, AT 2024ahwk, AT 2024aigt, AT 2024ahsx, AT 2024ahyq, and AT 2024aigv. We refer the reader to K. de Soto (2025, in preparation) for photometric analysis of AT 2024ahzi. Our transient search uses a subset of r-band images, which may not always optimally cover individual objects. To obtain multiband and better temporal coverage for specific objects, we search all DP1 images that overlap with each object's position and select up to two images per night per filter (to reduce computational cost). We then generated difference images and extracted photometry from 1500 × 1500 pixel cutouts centered on each object using SLIDE across all filters. Since there are no u-band observations in DES and few y-band observations in DP1, we performed image subtraction only on the $griz$-band images. The light curves and host properties of these objects are shown in Figure 2.

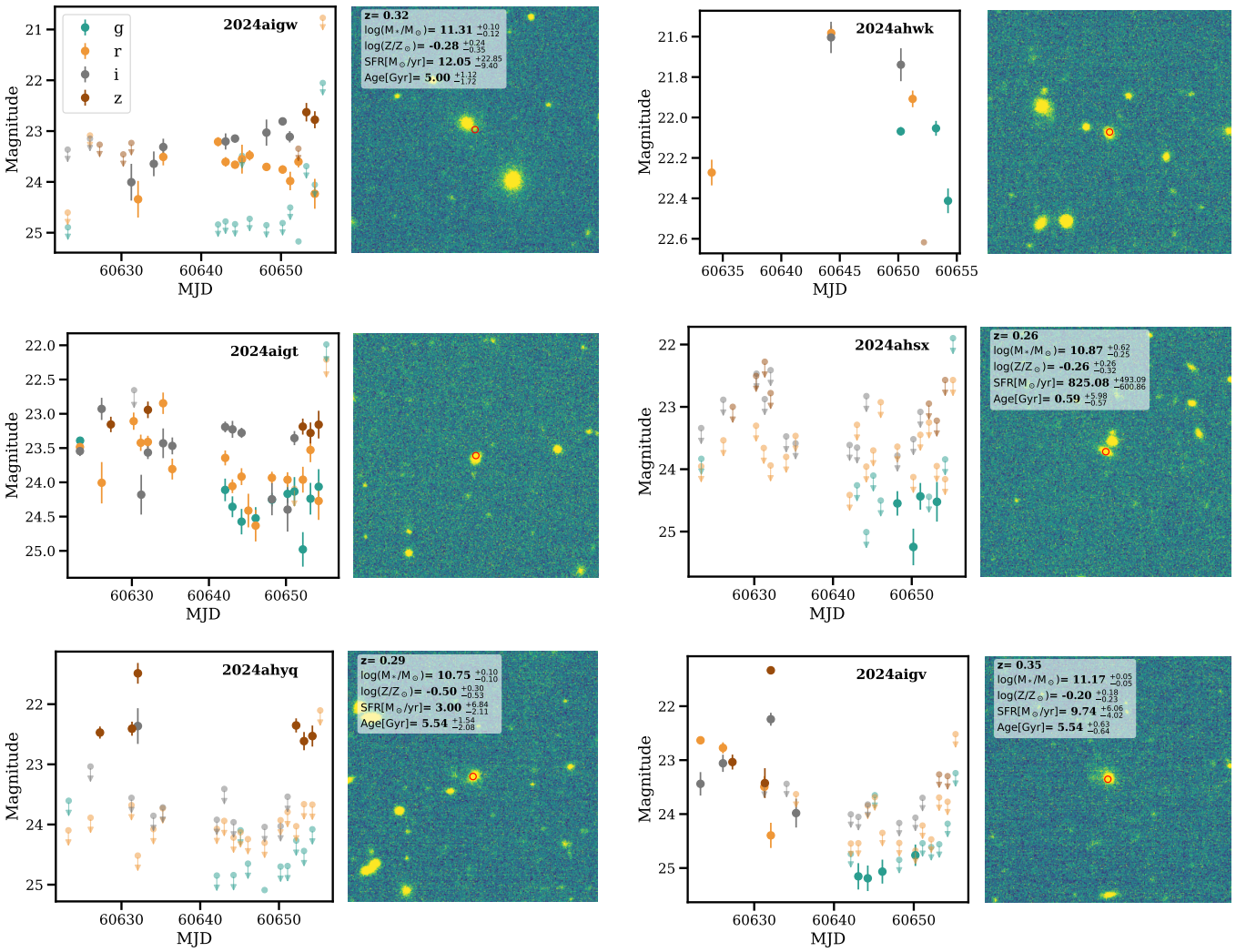

Figure 2. (Continued.)

3.3.2. *Unreported Transients*

We cross-match the remaining 29 candidates with the `DiaObject` table on the Rubin Science Platform, considering only `DiaObjects` with at least two detections. A total of 17 transients have a corresponding `DiaObject` within 1″. The remaining 12 transients are either missing or have less than two detections in the DP1 DIA catalog, because transient flux is contaminating the templates and pushing the difference flux variation below the detection threshold. This highlights the importance of robust templates in transient identification. We show examples of transients with and without `DiaObject` object associations in Figure 3.

3.4. *Host Properties of Transient Candidates*

In this Letter, we do not perform detailed light-curve analysis on our identified candidates; however, as a demonstration of the future workflow in the LSST era, we derive the host properties of each transient using `FrankenBlast` (A. E. Nugent et al. 2025), a customized version of `Blast` (D. O. Jones et al. 2024). `FrankenBlast` collects all available images of the host galaxies within the Galaxy Evolution Explorer (A. Y. K. Bouquin et al. 2018), Pan-STARRS1, DECaLS Data Release 9, Two Micron All-Sky Survey (M. F. Skrutskie et al. 2006), and Wide-field Infrared Survey Explorer (E. L. Wright et al. 2010). It then performs aperture photometry using elliptical apertures constructed for each image, using the `astropy.photutils` Python package (L. Bradley et al. 2025). If the host is not detected in a given filter, `FrankenBlast` adjusts the aperture size using a neighboring filter. Additional technical details are provided in the Appendix. Host properties of the transient candidates are presented in Tables 1 and 2, as well as in Figure 2. Host properties, especially photometric redshifts, can significantly improve the accuracy of photometric classifiers, particularly at early times (K. Boone 2019; D. Muthukrishna et al. 2019; S. Gomez et al. 2020; P. Sánchez-Sáez et al. 2021; A. Gagliano et al. 2023; M. Kisley et al. 2023; K. M. de Soto et al. 2024; X. Sheng et al. 2024; V. A. Villar et al. 2024; A. Boesky et al. 2025; R. Gupta et al. 2025).

4. Discussion and Conclusions

We present the `SLIDE` package, which performs LSST image subtraction using DECam templates. To demonstrate the anticipated workflow for the LSST survey, we conduct an experimental transient search via the Rubin Science Platform using DP1 difference images produced by this package. We

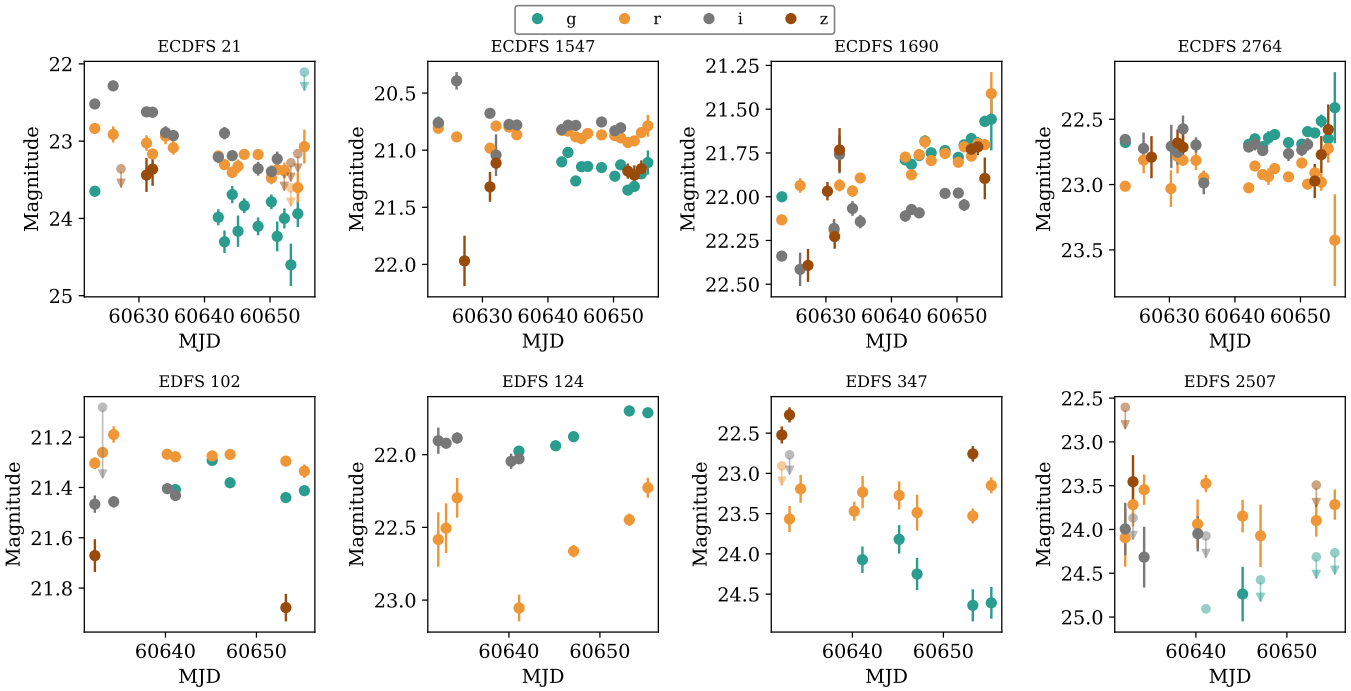

Figure 3. Multiband light curves of a subset of the transient candidates identified by our pipeline. More information about these transients can be found in Tables 1 and 2.

(The data used to create this figure are available in the online article.)

present multiband photometry and host galaxy properties for the most promising transients.

This Letter demonstrates the potential of SLIDE to uncover extended preexplosion or long-duration transient activity within LSST. In recent years, it has been found that many CCSNe, such as normal SNe II, SNe IIn, and SNe Ibn, interact with dense circumstellar material (CSM) around their progenitors (D. C. Leonard et al. 2000; N. Smith et al. 2015; D. Khazov et al. 2016; O. Yaron et al. 2017; A. Gangopadhyay et al. 2020, 2025; V. Morozova et al. 2020; S.-Q. Wang & L. Li 2020; R. J. Bruch et al. 2021, 2023; X. Wang et al. 2021; C. Pellegrino et al. 2022; G. Terreran et al. 2022; T. Ben-Ami et al. 2023; K. A. Bostroem et al. 2023a, 2023b; G. Hosseinzadeh et al. 2023; J. Pearson et al. 2023; J. E. Andrews et al. 2024, 2025; Y. Dong et al. 2024; W. V. Jacobson-Galán et al. 2024; N. Meza-Retamal et al. 2024; M. Shrestha et al. 2024a, 2024b; S. J. Brennan et al. 2025; Z. Y. Wang et al. 2025), likely produced months to years before their final explosions. The origin of this CSM, its geometry, and its implications for CCSN progenitor systems remain hotly debated (R. A. Chevalier 2012; E. Quataert & J. Shiode 2012; N. Soker 2013; J. H. Shiode & E. Quataert 2014; N. Smith & W. D. Arnett 2014; J. Fuller 2017; V. Morozova et al. 2020; L. Dessart et al. 2022; B. D. Metzger 2022; S. C. Wu & J. Fuller 2022; D. Tsuna et al. 2024a, 2024b).

Improved characterization of precursor emission provides critical insights into the final stages of stellar evolution, and may serve as an early warning signal for imminent CCSNe (D. Tsuna et al. 2023). To date, precursor activity has been most commonly observed in SNe IIn (N. L. Strotjohann et al. 2021; D. Farias et al. 2024; S. J. Brennan et al. 2025; A. Gagliano et al. 2025; A. Pastorello et al. 2025). In contrast, only three SNe Ibn (A. Pastorello et al. 2007; N. L. Strotjohann et al. 2021; S. J. Brennan et al. 2024; Y. Dong et al. 2024) and a single SN II (W. V. Jacobson-Galán et al. 2022) have shown evidence for precursor emission, potentially due to their fainter intrinsic luminosities. Moreover, precursor spectroscopy, critical for probing progenitor systems, has only been published for a few events (A. Pastorello et al. 2013; S. J. Brennan et al. 2024). Building a larger sample of SNe with detected precursor emission and precursor spectra is essential for constraining their occurrence rates and understanding their underlying physical mechanisms.

Furthermore, LSST is expected to drastically increase the number of photometrically identified, long-duration precursor events. With a single LSST visit, precursors from normal SNe II and SNe IIn can be detected to approximately 100 and 300 Mpc, respectively (W. V. Jacobson-Galán et al. 2022; A. Gagliano et al. 2025), while precursors of SNe Ibn can be detected to approximately 150 Mpc (e.g., Y. Dong et al. 2024). Therefore, precursor searches can be constrained to nearby, bright, low-extinction galaxies to reduce computational load and enable rapid identification and follow-up of promising candidates. Host association (e.g., with algorithms such as Pröst as we described in Section 3.2) is essential for targeted searches to further decrease the computational load on the Rubin Science Platform. Host galaxy properties can be derived using Blast and FrankenBlast, further enabling prioritization and classification. We expect SLIDE, paired with the approach outlined in this Letter, to be particularly effective in discovering these long-duration precursors.

Our package will support the study of all transients with slowly evolving phases. LRNe (J. C. Mauerhan et al. 2015; N. Smith et al. 2016; N. Blagorodnova et al. 2017), for example, are generally understood to be the product of common envelope episodes and, potentially, mergers (e.g., N. Soker & R. Tylenda 2003; R. Tylenda et al. 2011; B. D. Metzger & O. Pejcha 2017; N. Soker 2024). LRNe often undergo gradual brightening that lasts for years prior to the main outburst. Multiband photometric and spectroscopic observations during the preoutburst brightening phase can

Table 1
ECDFS Transient Candidates

ID	R.A. (hh:mm:ss)	Decl. (dd:mm:ss)	Nuc. Flag	$z_{\rm host}$	DIA Object ID	$\log(Z/Z_{\odot})$	$\log(M_{*}/M_{\odot})$	Age (Gyr)	SFR ($M_{\odot}$/yr)
Transients Reported to TNS									
2024ahsx	03:33:28.07	−28:12:54.36	1	0.261(0.011)	611253629533291776	$-0.26^{+0.26}_{-0.32}$	$10.87^{+0.62}_{-0.25}$	$0.59^{+5.98}_{-0.57}$	$825.08^{+493.09}_{-600.86}$
2024ahwk	03:29:50.944	−28:13:04.73	0	0.270(0.013)	611253973130674268	…	…	…	…
2024ahyq	03:31:37.65	−28:20:01.31	1	0.294(0.040)	609782139377943168	$-0.50^{+0.30}_{-0.53}$	$10.75^{+0.10}_{-0.10}$	$5.54^{+1.54}_{-2.08}$	$3.00^{+6.84}_{-2.11}$
2024ahyy	03:31:34.22	−28:24:45.37	0	0.438(0.105)	609781520902651904	$-0.80^{+0.54}_{-0.86}$	$9.67^{+0.28}_{-0.65}$	$3.54^{+1.57}_{-3.31}$	$8.24^{+7.07}_{-4.64}$
2024ahzc	03:31:21.18	−28:16:47.64	0	0.290(0.042)	609782208097419264	$-0.75^{+0.61}_{-0.72}$	$10.38^{+0.12}_{-0.13}$	$6.85^{+2.73}_{-0.92}$	$1.77^{+6.31}_{-1.27}$
2024aigg	03:32:29.94	−27:44:23.33	0	0.069(0.015)	611255759837069440	$-0.73^{+0.32}_{-0.43}$	$10.26^{+0.11}_{-0.09}$	$3.94^{+1.57}_{-1.86}$	$1.49^{+1.52}_{-0.76}$
2024aigj	03:32:51.02	−27:40:52.60	0	0.251(0.047)	611256447031836800	…	…	…	…
2024aigt	03:33:41.37	−28:13:24.81	0	0.296(0.053)	611253629533290624	…	…	…	…
2024aigw	03:30:55.57	−27:51:58.87	0	0.323(0.011)	611255210081255575	$-0.28^{+0.24}_{-0.35}$	$11.31^{+0.10}_{-0.12}$	$5.00^{+1.12}_{-1.72}$	$12.05^{+22.85}_{-9.40}$
2024aigv	03:32:13.81	−28:28:14.40	0	0.375(0.055)	609788942606139423	$-0.20^{+0.18}_{-0.23}$	$11.17^{+0.05}_{-0.05}$	$5.54^{+0.63}_{-0.64}$	$9.74^{+6.06}_{-4.03}$
Unreported Transients									
13	03:31:37.69	−28:04:10.16	0	0.132(0.020)	…	$-0.91^{+0.55}_{-0.47}$	$10.10^{+0.09}_{-0.11}$	$5.87^{+1.11}_{-1.66}$	$1.51^{+2.16}_{-0.80}$
14	03:31:35.11	−28:07:14.42	0	0.127(0.030)	611254522886494620	$-1.20^{+0.58}_{-0.45}$	$9.83^{+0.15}_{-0.21}$	$4.79^{+1.64}_{-4.10}$	$1.60^{+3.01}_{-0.98}$
21	03:31:41.65	−28:05:10.74	1	0.205(0.056)	611254454167011721	$-0.70^{+0.75}_{-0.74}$	$9.63^{+0.26}_{-0.68}$	$5.55^{+1.86}_{-5.29}$	$3.46^{+8.91}_{-2.61}$
100	03:31:34.14	−27:49:59.61	0	0.464(0.125)	…	$-1.06^{+0.72}_{-0.61}$	$10.21^{+0.21}_{-0.77}$	$3.35^{+1.45}_{-3.29}$	$34.04^{+37.63}_{-20.92}$
706	03:33:32.49	−27:48:32.00	1	0.333(0.108)	…	$-0.76^{+0.66}_{-0.88}$	$9.64^{+0.36}_{-0.72}$	$3.99^{+1.82}_{-3.87}$	$7.05^{+9.50}_{-4.86}$
1071	03:31:41.92	−28:04:22.22	0	0.149(0.033)	…	$-0.69^{+0.63}_{-0.79}$	$9.41^{+0.22}_{-0.65}$	$4.82^{+2.42}_{-4.79}$	$3.54^{+11.21}_{-2.98}$
1314	03:33:07.70	−27:53:31.81	1	0.121(0.036)	…	$-0.85^{+0.71}_{-0.65}$	$9.21^{+0.13}_{-0.20}$	$6.27^{+1.42}_{-2.76}$	$0.32^{+1.26}_{-0.19}$
1350	03:32:49.30	−27:37:57.07	1	0.131(0.066)	611256447031837444	…	…	…	…
1367	03:33:21.09	−27:39:12.07	1	0.597(0.298)	611256378312359976	…	…	…	…
1547	03:32:46.03	−28:22:32.21	1	0.621(0.216)	609788873886662802	$-0.47^{+0.44}_{-0.53}$	$10.59^{+0.25}_{-0.63}$	$3.74^{+1.08}_{-3.65}$	$82.07^{+91.77}_{-45.82}$
1690	03:31:20.77	−27:56:49.26	1	0.834(0.118)	611255210081255450	$-0.37^{+0.35}_{-0.81}$	$10.39^{+0.16}_{-0.25}$	$3.07^{+0.70}_{-1.48}$	$14.58^{+8.55}_{-5.80}$
1897	03:33:09.50	−27:44:06.89	1	0.117(0.032)	611255691117594961	…	…	…	…
1965	03:31:24.22	−27:53:42.27	1	0.110(0.055)	611255210081255504	…	…	…	…
2764	03:31:47.87	−28:17:00.77	1	1.130(0.231)	…	$-0.16^{+0.22}_{-0.34}$	$11.62^{+0.10}_{-0.10}$	$3.08^{+0.48}_{-1.19}$	$6.19^{+18.46}_{-4.86}$
2798	03:33:46.01	−28:20:07.43	1	0.170(0.038)	…	$-0.75^{+0.53}_{-0.69}$	$9.41^{+0.19}_{-0.32}$	$4.97^{+1.61}_{-3.83}$	$1.16^{+2.44}_{-0.77}$

Note: Galaxy properties are not derived for hosts with insufficient photometric data.

Table 2
EDFS Transient Candidates

ID	R.A. (hh:mm:ss)	Decl. (dd:mm:ss)	Nuc. Flag	$z_{\rm host}$	DIA Object ID	$\log(Z/Z_{\odot})$	$\log(M_{*}/M_{\odot})$	Age (Gyr)	SFR ($M_{\odot}$/yr)
				Transients Reported to TNS					
2024aigh	03:57:17.80	−48:22:08.30	0	0.06(0.04)	592915218690999552	$-0.45^{+0.25}_{-0.21}$	$10.66^{+0.51}_{-1.28}$	$7.75^{+1.63}_{-0.77}$	$0.03^{+0.12}_{-0.03}$
2024aigk	03:55:31.82	−48:27:43.71	1	0.168(0.030)	592915356129952000	$-0.17^{+0.27}_{-0.64}$	$10.16^{+0.27}_{-0.50}$	$1.83^{+3.76}_{-1.62}$	$3.03^{+13.04}_{-2.91}$
2024aigl	03:59:24.16	−48:46:50.53	0	0.225(0.021)	592913706862510093	$-0.75^{+0.46}_{-0.45}$	$10.49^{+0.09}_{-0.12}$	$5.26^{+1.09}_{-2.45}$	$4.44^{+5.94}_{-2.54}$
2024aigs	03:56:53.23	−49:06:18.06	0	0.393(0.147)	591819074317582336	$-0.74^{+0.75}_{-0.68}$	$10.03^{+0.13}_{-0.27}$	$4.89^{+0.89}_{-2.12}$	$5.59^{+7.39}_{-2.94}$
				Unreported Transients					
102	03:57:09.25	−48:47:02.21	1	0.987(0.105)	592913844301464254	$-0.02^{+0.15}_{-0.25}$	$10.96^{+0.40}_{-0.51}$	$1.17^{+1.67}_{-1.09}$	$416.87^{+291.91}_{-207.38}$
124	03:56:23.21	−48:21:48.14	1	0.637(0.076)	592915287410475027	$-0.25^{+0.24}_{-0.29}$	$11.12^{+0.31}_{-0.54}$	$3.68^{+1.32}_{-3.62}$	$281.54^{+329.42}_{-183.53}$
199	03:56:48.54	−48:19:13.44	1	0.148(0.017)	592915974605242521	…	…	…	…
206	03:57:28.37	−48:27:49.38	0	0.156(0.040)	592915218690998834	$-0.29^{+0.24}_{-0.35}$	$10.85^{+0.06}_{-0.07}$	$6.41^{+0.86}_{-0.98}$	$2.51^{+2.75}_{-1.31}$
347	03:54:35.18	−48:43:37.65	0	0.367(0.141)	592914050459894637	$-0.45^{+0.40}_{-0.85}$	$10.53^{+0.20}_{-0.29}$	$5.17^{+1.51}_{-4.16}$	$7.61^{+20.32}_{-5.86}$
357	03:54:15.75	−48:35:30.15	0	1.112(0.202)	592914737654661956	$0.07^{+0.09}_{-0.20}$	$10.73^{+0.26}_{-0.14}$	$0.04^{+1.68}_{-0.03}$	$842.01^{+317.67}_{-244.37}$
392	03:57:16.36	−48:51:04.92	1	0.829(0.240)	592913157106705461	$-1.24^{+0.45}_{-0.34}$	$11.29^{+0.14}_{-0.27}$	$0.51^{+0.64}_{-0.25}$	$133.94^{+204.08}_{-75.63}$
490	03:55:53.49	−48:22:19.23	1	0.574(0.205)	592915356129953233	…	…	…	…
569	03:57:27.61	−48:28:38.66	0	0.406(0.159)	…	…	…	…	…
668	03:56:41.15	−48:16:57.78	0	0.171(0.056)	…	$-0.84^{+0.63}_{-0.72}$	$10.34^{+0.19}_{-0.31}$	$5.17^{+1.61}_{-3.18}$	$2.13^{+4.01}_{-1.58}$
1236	03:58:16.51	−48:27:33.57	1	0.399(0.166)	…	$-0.61^{+0.45}_{-1.07}$	$9.68^{+0.20}_{-0.30}$	$5.16^{+0.89}_{-1.45}$	$2.56^{+1.61}_{-1.05}$
2507	03:56:00.29	−48:45:22.26	0	0.119(0.059)	…	$-0.67^{+0.60}_{-0.86}$	$8.99^{+0.22}_{-0.31}$	$5.65^{+2.05}_{-4.96}$	$0.14^{+0.51}_{-0.12}$
4777	03:55:53.52	−49:07:29.71	1	0.147(0.025)	591819143037059212	…	…	…	…
5575	03:54:41.14	−48:34:11.92	0	0.187(0.037)	…	$-0.68^{+0.44}_{-0.67}$	$9.84^{+0.18}_{-0.31}$	$5.18^{+1.57}_{-3.80}$	$4.96^{+9.11}_{-3.17}$

offer valuable information about their progenitor systems and mass transfer mechanisms preceding the transient (H. Addison et al. 2022). LSST is expected to observe ∼400–800 LRNe annually (G. Howitt et al. 2020), drastically increasing the current sample of such events.

Similarly, some extremely energetic transients often evolve slowly. Superluminous SNe, in particular, are a class of massive stellar explosions with luminosities significantly higher than those of normal SNe, requiring additional power sources beyond radioactive decay (A. Gal-Yam et al. 2009; L. Chomiuk et al. 2011; R. M. Quimby et al. 2011; A. Gal-Yam 2012; D. A. Howell et al. 2013; D. A. Howell 2017; T. J. Moriya et al. 2018; S. Gomez et al. 2024). LSST is expected to discover ∼10,000 hydrogen-poor superluminous events annually, with most at high redshift ($z > 1$; V. A. Villar et al. 2018). Similarly, ambiguous nuclear transients are energetic transients that are found in the nuclei of their host galaxies (P. J. Pessi et al. 2025; P. Wiseman et al. 2025). These are seemingly distinct from typical active galactic nuclei (AGN) and notably more extreme than "normal" tidal disruption events, although their origin is still an open question. In both cases, the extended duration of these events, especially at high redshift, implies that they are likely to be implanted in the initial LSST templates.

Early identification of transient events is essential for spectroscopic follow-up across their evolution. `SLIDE` enables both early detection and reliable photometry, even when the transients are embedded in their LSST template images. Because the aforementioned transient classes are rare, the early years of LSST offer an opportunity to build statistically meaningful samples of such events that will guide strategies for follow-up in the future.

Acknowledgments

We thank Griffin Hosseinzadeh for providing the PyZOGY image subtraction example. We thank Gautham Narayan, Tanner Murphey, and Qinan Wang for helpful discussions. We also thank Padma Venkatraman for testing the package and providing valuable feedback.

The Villar Astro Time Lab acknowledges support through the David and Lucile Packard Foundation, the Research Corporation for Scientific Advancement (through a Cottrell Fellowship), the National Science Foundation under AST-2433718, AST-2407922, and AST-2406110, as well as an Aramont Fellowship for Emerging Science Research. This work is supported by the National Science Foundation under Cooperative Agreement PHY-2019786 (the NSF AI Institute for Artificial Intelligence and Fundamental Interactions). K.d.S. thanks the LSST-DA Data Science Fellowship Program, which is funded by LSST-DA, the Brinson Foundation, the WoodNext Foundation, and the Research Corporation for Science Advancement Foundation; her participation in the program has benefited this work.

This research made use of Photutils, an Astropy package for detection and photometry of astronomical sources (L. Bradley et al. 2022).

This research uses services or data provided by the Astro Data Lab, which is part of the Community Science and Data Center (CSDC) Program of NSF NOIRLab. NOIRLab is operated by the Association of Universities for Research in Astronomy (AURA), Inc. under a cooperative agreement with the U.S. National Science Foundation.

This work has made use of data from the European Space Agency (ESA) mission Gaia (https://www.cosmos.esa.int/gaia), processed by the Gaia Data Processing and Analysis Consortium (DPAC; https://www.cosmos.esa.int/web/gaia/dpac/consortium). Funding for the DPAC has been provided by national institutions, in particular the institutions participating in the Gaia Multilateral Agreement.

Facilities: ADS, Astro Data Lab, Rubin:Simonyi (LSSTComCam), Rubin:USDAC.

Software: Astropy (Astropy Collaboration et al. 2013, 2018, 2022), `Pröst` (A. Gagliano et al. 2025), Matplotlib (J. D. Hunter 2007), NumPy (C. R. Harris et al. 2020), Pandas (W. McKinney 2010), SciPy (P. Virtanen et al. 2020), Butler (T. Jenness et al. 2022), Photutils (L. Bradley et al. 2025).

Appendix
`FrankenBlast` Stellar Population Modeling

`FrankenBlast` constrains host galaxy stellar population properties using `SBI++`, a simulation-based inference technique that learns posterior density distributions of stellar population properties from simulated galaxy photometry (B. Wang et al. 2023). `FrankenBlast` trains its model on 2 million simulated galaxies from `Prospector` (J. Leja et al. 2019; B. D. Johnson et al. 2021), a stellar population modeling inference code, which uses `FSPS` and `python-FSPS` (C. Conroy et al. 2009; C. Conroy & J. E. Gunn 2010) to create mock photometry from a given set of stellar population properties. The mock photometry is noised up to match the SNR of the observed sources within the aforementioned surveys used for photometry. `FrankenBlast` employs the G. Chabrier (2003) initial mass function, the M. Kriek & C. Conroy (2013) dust attenuation model and B. T. Draine & A. Li (2007) IR dust extinction model, a nebular emission model (N. Byler et al. 2017), and an AGN mid-IR model within its `Prospector` model. It tracks the star formation history (SFH) of the hosts through a seven-bin nonparametric model. This SFH model assumes a constant star formation rate (SFR) in a single age bin: the first two age bins are linearly spaced from 0 to 30 Myr and 30–100 Myr, and the final five are log-spaced until the age of the Universe at the host's redshift (or sampled redshift, if it is not known). We report present-day SFR as the SFR in the first two age bins. For accurate constraints on stellar metallicity, `FrankenBlast` includes the A. Gallazzi et al. (2005) mass–metallicity relation. When fitting the observed host galaxy data, we have the option to set the host's redshift at a specific value (spec-z model), or sample redshift as a fit parameter (photo-z model; assumes $0 \leqslant z \leqslant 1.5$). If a spectroscopic or photometric redshift estimate of the host galaxy is given from the `Pröst` host association (see Section 3.1), we use that redshift as the redshift of the host and fit with the spec-z model. Otherwise, redshift is determined through the photo-z model.

ORCID iDs

Yize Dong (董一泽) https://orcid.org/0000-0002-7937-6371
Kaylee de Soto https://orcid.org/0000-0002-9886-2834
V. Ashley Villar https://orcid.org/0000-0002-5814-4061
Anya Nugent https://orcid.org/0000-0002-2028-9329
Alex Gagliano https://orcid.org/0000-0003-4906-8447
K. Azalee Bostroem https://orcid.org/0000-0002-4924-444X
Anastasia Alexov https://orcid.org/0009-0000-7835-3963

Éric Aubourg https://orcid.org/0000-0002-5592-023X
Farrukh Azfar https://orcid.org/0000-0002-4052-2511
Alexandre Boucaud https://orcid.org/0000-0001-7387-2633
Johann Cohen-Tanugi https://orcid.org/0000-0001-9022-4232
Sylvie Dagoret-Campagne https://orcid.org/0000-0003-1131-7030
Holger Drass https://orcid.org/0000-0002-7790-9971
Orion Eiger https://orcid.org/0000-0003-2933-391X
Leanne P. Guy https://orcid.org/0000-0003-0800-8755
Željko Ivezić https://orcid.org/0000-0001-5250-2633
M. James Jee https://orcid.org/0000-0002-5751-3697
Tim Jenness https://orcid.org/0000-0001-5982-167X
Steven M. Kahn https://orcid.org/0000-0003-4833-9137
Yijung Kang https://orcid.org/0000-0002-5261-5803
Lee S. Kelvin https://orcid.org/0000-0001-9395-4759
Gábor Kovács https://orcid.org/0000-0003-1779-775X
Laurent Le Guillou https://orcid.org/0000-0001-7178-8868
Mostafa Lutfi https://orcid.org/0000-0003-2866-3802
Guillem Megias Homar https://orcid.org/0000-0001-6013-1131
Erfan Nourbakhsh https://orcid.org/0000-0003-3827-4691
Hye Yun Park https://orcid.org/0000-0002-7295-2743
John R. Peterson https://orcid.org/0000-0001-5471-9609
Andrés A. Plazas Malagón https://orcid.org/0000-0002-2598-0514
Daniel Polin https://orcid.org/0000-0001-7445-4724
Bruno C. Quint https://orcid.org/0000-0002-1557-3560
Tiago Ribeiro https://orcid.org/0000-0002-0138-1365
Vincent J. Riot https://orcid.org/0000-0001-8239-3079
Cécile Roucelle https://orcid.org/0000-0002-9641-4552
Bruno O. Sánchez https://orcid.org/0000-0002-8687-0669
David Sanmartim https://orcid.org/0000-0002-9238-9521
Nima Sedaghat https://orcid.org/0000-0003-4734-2019
Richard A. Shaw https://orcid.org/0000-0003-4058-5202
Alysha Shugart https://orcid.org/0009-0000-6778-7168
Ioana Sotuela Elorriaga https://orcid.org/0009-0001-6379-3365
Krzysztof Suberlak https://orcid.org/0000-0002-9589-1306
John D. Swinbank https://orcid.org/0000-0001-9445-1846
Sandrine Thomas https://orcid.org/0000-0002-9121-3436
J. Anthony Tyson https://orcid.org/0000-0002-9242-8797
Wouter van Reeven https://orcid.org/0000-0002-1431-9245
Charlotte Ward https://orcid.org/0000-0002-4557-6682
Christopher Z. Waters https://orcid.org/0000-0003-1989-4879
W. M. Wood-Vasey https://orcid.org/0000-0001-7113-1233

References

Abbott, T. M. C., Adamów, M., Aguena, M., et al. 2021, ApJS, 255, 20
Addison, H., Blagorodnova, N., Groot, P. J., et al. 2022, MNRAS, 517, 1884
Aleo, P. D., Malanchev, K., Sharief, S., et al. 2023, ApJS, 266, 9
Andreoni, I., Freeburn, J., Carney, J., Anumarlapudi, A., & Teague, S. 2025, TNSAN, 204, 1
Andrews, J. E., Pearson, J., Hosseinzadeh, G., et al. 2024, ApJ, 965, 85
Andrews, J. E., Shrestha, M., Bostroem, K. A., et al. 2025, ApJ, 980, 37
Anumarlapudi, A., Freeburn, J., Carney, J., Teague, S., & Andreoni, I. 2025, TNSTR, 2025-2552, 1
Astropy Collaboration, Price-Whelan, A. M., Lim, P. L., et al. 2022, ApJ, 935, 167
Astropy Collaboration, Price-Whelan, A. M., Sipőcz, B. M., et al. 2018, AJ, 156, 123
Astropy Collaboration, Robitaille, T. P., Tollerud, E. J., et al. 2013, A&A, 558, A33
Barbary, K. 2016, JOSS, 1, 58
Ben-Ami, T., Arcavi, I., Newsome, M., et al. 2023, ApJ, 946, 30
Bertin, E., & Arnouts, S. 1996, A&AS, 117, 393
Bianco, F. B., Ivezić, Ž., Jones, R. L., et al. 2022, ApJS, 258, 1
Blagorodnova, N., Kotak, R., Polshaw, J., et al. 2017, ApJ, 834, 107
Blum, R. D., Burleigh, K., Dey, A., et al. 2016, AAS Meeting, 228, 317.01
Boesky, A., Villar, V. A., Gagliano, A., & Hsu, B. 2025, arXiv:2506.00121
Boone, K. 2019, AJ, 158, 257
Bostroem, K. A., Dessart, L., Hillier, D. J., et al. 2023b, ApJL, 953, L18
Bostroem, K. A., Pearson, J., Shrestha, M., et al. 2023a, ApJL, 956, L5
Bouquin, A. Y. K., Gil de Paz, A., Muñoz-Mateos, J. C., et al. 2018, ApJS, 234, 18
Bradley, L., Sipőcz, B., Robitaille, T., et al. 2022, astropy/photutils, v1.5.0, Zenodo, doi:10.5281/zenodo.6825092
Bradley, L., Sipőcz, B., Robitaille, T., et al. 2025, astropy/photutils, v2.2.0, Zenodo, doi:10.5281/zenodo.596036
Brennan, S. J., Barmentloo, S., Schulze, S., et al. 2025, arXiv:2503.08768
Brennan, S. J., Sollerman, J., Irani, I., et al. 2024, A&A, 684, L18
Bruch, R. J., Gal-Yam, A., Schulze, S., et al. 2021, ApJ, 912, 46
Bruch, R. J., Gal-Yam, A., Yaron, O., et al. 2023, ApJ, 952, 119
Byler, N., Dalcanton, J. J., Conroy, C., & Johnson, B. D. 2017, ApJ, 840, 44
Chabrier, G. 2003, PASP, 115, 763
Chambers, K. C., Magnier, E. A., Metcalfe, N., et al. 2016, arXiv:1612.05560
Chevalier, R. A. 2012, ApJL, 752, L2
Chomiuk, L., Chornock, R., Soderberg, A. M., et al. 2011, ApJ, 743, 114
Conroy, C., & Gunn, J. E. 2010, ApJ, 712, 833
Conroy, C., Gunn, J. E., & White, M. 2009, ApJ, 699, 486
Dálya, G., Díaz, R., Bouchet, F. R., et al. 2022, MNRAS, 514, 1403
Dark Energy Survey Collaboration, Abbott, T., Abdalla, F. B., et al. 2016, MNRAS, 460, 1270
de Soto, K. M., Villar, V. A., Berger, E., et al. 2024, ApJ, 974, 169
DeForest, C. E. 2004, SoPh, 219, 3
Dessart, L., Hillier, D. J., & Kuncarayakti, H. 2022, A&A, 658, A130
Dey, A., Schlegel, D. J., Lang, D., et al. 2019, AJ, 157, 168
Dong, Y., Tsuna, D., Valenti, S., et al. 2024, ApJ, 977, 254
Draine, B. T., & Li, A. 2007, ApJ, 657, 810
Dubois-Felsmann, G., Economou, F., Lim, K.-T., et al. 2019, Science Platform Design, Vera C. Rubin Observatory Data Management Controlled Document LDM-542, https://ldm-542.lsst.io/LDM-542.pdf
Farias, D., Gall, C., Narayan, G., et al. 2024, ApJ, 977, 152
Fitzpatrick, M. J., Olsen, K., Economou, F., et al. 2014, Proc. SPIE, 9149, 91491T
Flaugher, B., Diehl, H. T., Honscheid, K., et al. 2015, AJ, 150, 150
Flewelling, H. A., Magnier, E. A., Chambers, K. C., et al. 2020, ApJS, 251, 7
Freeburn, J., Andreoni, I., Anumarlapudi, A., Carney, J., & Teague, S. 2025a, TNSTR, 2025-2796, 1
Freeburn, J., Andreoni, I., Anumarlapudi, A., Carney, J., & Teague, S. 2025b, TNSTR, 2025-2822, 1
Freeburn, J., Andreoni, I., Anumarlapudi, A., Carney, J., & Teague, S. 2025c, TNSTR, 2025-2862, 1
Freeburn, J., Andreoni, I., de Soto, K. M., et al. 2025d, arXiv:2507.22864
Freeburn, J., Carney, J., Anumarlapudi, A., Teague, S., & Andreoni, I. 2025e, TNSTR, 2025-2522, 1
Freeburn, J., Carney, J., Anumarlapudi, A., Teague, S., & Andreoni, I. 2025f, TNSTR, 2025-2519, 1
Freeburn, J., Teague, S., Carney, J., Anumarlapudi, A., & Andreoni, I. 2025g, TNSTR, 2025-2533, 1
Fuller, J. 2017, MNRAS, 470, 1642
Gagliano, A., Berger, E., Villar, V. A., et al. 2025, ApJ, 978, 110
Gagliano, A., Contardo, G., Foreman-Mackey, D., Malz, A. I., & Aleo, P. D. 2023, ApJ, 954, 6
Gagliano, A., de Soto, K., Boesky, A., & Manning, T. A. 2025, alexandergagliano/Prost, v1.2.11, Zenodo, doi:10.5281/zenodo.15397886
Gagliano, A., Villar, V. A., Matsumoto, T., et al. 2025, ApJ, 989, 182
Gaia Collaboration, Brown, A. G. A., Vallenari, A., et al. 2021, A&A, 649, A1
Gaia Collaboration, Prusti, T., de Bruijne, J. H. J., et al. 2016, A&A, 595, A1
Gal-Yam, A. 2012, Sci, 337, 927
Gal-Yam, A. 2021, AAS Meeting, 53, 423.05
Gal-Yam, A., Mazzali, P., Ofek, E. O., et al. 2009, Natur, 462, 624
Gallazzi, A., Charlot, S., Brinchmann, J., White, S. D. M., & Tremonti, C. A. 2005, MNRAS, 362, 41
Gangopadhyay, A., Misra, K., Hiramatsu, D., et al. 2020, ApJ, 889, 170
Gangopadhyay, A., Sollerman, J., Tsalapatas, K., et al. 2025, MNRAS, Advance Access

Gomez, S. 2024, iinuclear: Nuclear Transient Classifier, GitHub, https://github.com/gmzsebastian/iinuclear
Gomez, S., Berger, E., Blanchard, P. K., et al. 2020, ApJ, 904, 74
Gomez, S., Nicholl, M., Berger, E., et al. 2024, MNRAS, 535, 471
Guevel, D., & Hosseinzadeh, G. 2017, dguevel/PyZOGY: Initial release, v0.0.1, Zenodo, doi:10.5281/zenodo.1043973
Gupta, R., Muthukrishna, D., Rehemtulla, N., & Shah, V. 2025, MNRAS, 542, L132
Guy, L. P., Bechtol, K., Bellm, E., et al. 2023, Rubin Observatory Plans for an Early Science Program, RTN-011, v5.0, Zenodo, doi:10.5281/zenodo.10059624
Guy, L. P., Bechtol, K., Bellm, E., et al. 2025, Rubin Technical Note RTN-011, NSF-DOE Vera C. Rubin Observatory
Harris, C. R., Millman, K. J., van der Walt, S. J., et al. 2020, Natur, 585, 357
Honscheid, K., & DePoy, D. L. 2008, arXiv:0810.3600
Hosseinzadeh, G., Farah, J., Shrestha, M., et al. 2023, ApJL, 953, L16
Howell, D. A. 2017, in Handbook of Supernovae, ed. A. W. Alsabti & P. Murdin, 431
Howell, D. A., Kasen, D., Lidman, C., et al. 2013, ApJ, 779, 98
Howitt, G., Stevenson, S., Vigna-Gómez, A., et al. 2020, MNRAS, 492, 3229
Hunter, J. D. 2007, CSE, 9, 90
Ivezić, Ž., Kahn, S. M., Tyson, J. A., et al. 2019, ApJ, 873, 111
Jacobson-Galán, W. V., Dessart, L., Davis, K. W., et al. 2024, ApJ, 970, 189
Jacobson-Galán, W. V., Dessart, L., Jones, D. O., et al. 2022, ApJ, 924, 15
Jenness, T., Bosch, J. F., Salnikov, A., et al. 2022, Proc. SPIE, 12189, 1218911
Johnson, B. D., Leja, J., Conroy, C., & Speagle, J. S. 2021, ApJS, 254, 22
Jones, D. O., Foley, R. J., Narayan, G., et al. 2021, ApJ, 908, 143
Jones, D. O., McGill, P., Manning, T. A., et al. 2024, arXiv:2410.17322
Khazov, D., Yaron, O., Gal-Yam, A., et al. 2016, ApJ, 818, 3
Kisley, M., Qin, Y.-J., Zabludoff, A., Barnard, K., & Ko, C.-L. 2023, ApJ, 942, 29
Kriek, M., & Conroy, C. 2013, ApJL, 775, L16
Leja, J., Johnson, B. D., Conroy, C., et al. 2019, ApJ, 877, 140
Leonard, D. C., Filippenko, A. V., Barth, A. J., & Matheson, T. 2000, ApJ, 536, 239
LSST Science Collaboration, Abell, P. A., Allison, J., et al. 2009, arXiv:0912.0201
Mauerhan, J. C., Van Dyk, S. D., Graham, M. L., et al. 2015, MNRAS, 447, 1922
McKinney, W. 2010, in Proc. 9th Python in Science Conf., ed. S. van der Walt & J. Millman, 56
Metzger, B. D. 2022, ApJ, 932, 84
Metzger, B. D., & Pejcha, O. 2017, MNRAS, 471, 3200
Meza-Retamal, N., Dong, Y., Bostroem, K. A., et al. 2024, ApJ, 971, 141
Moriya, T. J., Sorokina, E. I., & Chevalier, R. A. 2018, SSRv, 214, 59
Morozova, V., Piro, A. L., Fuller, J., & Van Dyk, S. D. 2020, ApJL, 891, L32
Murphey, C. T., Nair, G., Narayan, G., et al. 2025, TNSTR, 2025-975, 1
Muthukrishna, D., Narayan, G., Mandel, K. S., Biswas, R., & Hložek, R. 2019, PASP, 131, 118002
Nikutta, R., Fitzpatrick, M., Scott, A., & Weaver, B. 2020, A&C, 33, 100411
NSF-DOE Vera C. Rubin Observatory 2025a, Rubin Technical Note RTN-095, NSF-DOE Vera C. Rubin Observatory
NSF-DOE Vera C. Rubin Observatory 2025b, Legacy Survey of Space and Time Data Preview 1, NSF-DOE Vera C. Rubin Observatory, doi:10.71929/RUBIN/2570308
NSF-DOE Vera C. Rubin Observatory 2025c, LSST,
Nugent, A. E., Villar, V. A., Gagliano, A., et al. 2025, arXiv:2509.08874
O'Mullane, W., Economou, F., Huang, F., et al. 2024, in ASP Conf. Ser. 535, Astromical Data Analysis Software and Systems XXXI, ed. B. V. Hugo, R. Van Rooyen, & O. M. Smirnov (San Francisco, CA: ASP), 227
Pastorello, A., Cappellaro, E., Inserra, C., et al. 2013, ApJ, 767, 1
Pastorello, A., Reguitti, A., Tartaglia, L., et al. 2025, A&A, 701, A32
Pastorello, A., Smartt, S. J., Mattila, S., et al. 2007, Natur, 447, 829
Pearson, J., Hosseinzadeh, G., Sand, D. J., et al. 2023, ApJ, 945, 107
Pellegrino, C., Howell, D. A., Vinkó, J., et al. 2022, ApJ, 926, 125
Pessi, P. J., Lunnan, R., Sollerman, J., et al. 2025, MNRAS, 542, 3354
Quataert, E., & Shiode, J. 2012, MNRAS, 423, L92
Quimby, R. M., Kulkarni, S. R., Kasliwal, M. M., et al. 2011, Natur, 474, 487
Riello, M., De Angeli, F., Evans, D. W., et al. 2021, A&A, 649, A3
Rubin Observatory Science Pipelines Developers 2025, The LSST Science Pipelines Software: Optical Survey Pipeline Reduction and Analysis Environment PSTN-019, NSF-DOE Vera C. Rubin Observatory
Sánchez-Sáez, P., Reyes, I., Valenzuela, C., et al. 2021, AJ, 161, 141
Sheng, X., Nicholl, M., Smith, K. W., et al. 2024, MNRAS, 531, 2474
Shiode, J. H., & Quataert, E. 2014, ApJ, 780, 96
Shrestha, M., Bostroem, K. A., Sand, D. J., et al. 2024a, ApJL, 972, L15
Shrestha, M., Pearson, J., Wyatt, S., et al. 2024b, ApJ, 961, 247
Skrutskie, M. F., Cutri, R. M., Stiening, R., et al. 2006, AJ, 131, 1163
SLAC National Accelerator LaboratoryNSF-DOE Vera C. Rubin Observatory 2024, LSST Commissioning Camera, SLAC National Accelerator Laboratory (SLAC) (Menlo Park, CA: SLAC National Accelerator Laboratory (SLAC))
SLAC National Accelerator LaboratoryNSF-DOE Vera C. Rubin Observatory 2025, SLAC National Accelerator Laboratory and NSF-DOE Vera C. Rubin Observatory 2025 The LSST Camera (LSSTCam) (Menlo Park, CA: SLAC National Accelerator Laboratory (SLAC))
Smith, N., Andrews, J. E., Van Dyk, S. D., et al. 2016, MNRAS, 458, 950
Smith, N., & Arnett, W. D. 2014, ApJ, 785, 82
Smith, N., Mauerhan, J. C., Cenko, S. B., et al. 2015, MNRAS, 449, 1876
Soker, N. 2013, arXiv:1302.5037
Soker, N. 2024, Galax, 12, 33
Soker, N., & Tylenda, R. 2003, ApJL, 582, L105
Strotjohann, N. L., Ofek, E. O., Gal-Yam, A., et al. 2021, ApJ, 907, 99
Terreran, G., Jacobson-Galán, W. V., Groh, J. H., et al. 2022, ApJ, 926, 20
Tsuna, D., Matsumoto, T., Wu, S. C., & Fuller, J. 2024a, ApJ, 966, 30
Tsuna, D., Takei, Y., & Shigeyama, T. 2023, ApJ, 945, 104
Tsuna, D., Wu, S. C., Fuller, J., Dong, Y., & Piro, A. L. 2024b, OJAp, 7, 82
Tylenda, R., Hajduk, M., Kamiński, T., et al. 2011, A&A, 528, A114
Villar, V. A., Gomez, S., Berger, E., & Gagliano, A. 2024, ApJS, 276, 3
Villar, V. A., Nicholl, M., & Berger, E. 2018, ApJ, 869, 166
Virtanen, P., Gommers, R., Oliphant, T. E., et al. 2020, NatMe, 17, 261
Wang, B., Leja, J., Villar, V. A., & Speagle, J. S. 2023, ApJL, 952, L10
Wang, S.-Q., & Li, L. 2020, ApJ, 900, 83
Wang, X., Lin, W., Zhang, J., et al. 2021, ApJ, 917, 97
Wang, Z. Y., Pastorello, A., Cai, Y. Z., et al. 2025, A&A, 700, A156
Wiseman, P., Williams, R. D., Arcavi, I., et al. 2025, MNRAS, 537, 2024
Wright, E. L., Eisenhardt, P. R. M., Mainzer, A. K., et al. 2010, AJ, 140, 1868
Wu, S. C., & Fuller, J. 2022, ApJL, 940, L27
Yaron, O., Perley, D. A., Gal-Yam, A., et al. 2017, NatPh, 13, 510
Zackay, B., Ofek, E. O., & Gal-Yam, A. 2016, ApJ, 830, 27